analytical chemistry

pubs.acs.org/ac

Article

Raman Spectroscopy to Monitor Post-Translational Modifications and Degradation in Monoclonal Antibody Therapeutics

Bethan S. McAvan, Leo A. Bowsher, Thomas Powell, John F. O'Hara, Mariangela Spitali, Royston Goodacre, and Andrew J. Doig*

Cite This: *Anal. Chem.* 2020, 92, 10381−10389

Read Online

ACCESS | Metrics & More | Article Recommendations | Supporting Information

ABSTRACT: Monoclonal antibodies (mAbs) represent a rapidly expanding market for biotherapeutics. Structural changes in the mAb can lead to unwanted immunogenicity, reduced efficacy, and loss of material during production. The pharmaceutical sector requires new protein characterization tools that are fast, applicable in situ and to the manufacturing process. Raman has been highlighted as a technique to suit this application as it is information-rich, minimally invasive, insensitive to water background and requires little to no sample preparation. This study investigates the applicability of Raman to detect Post-Translational Modifications (PTMs) and degradation seen in mAbs. IgG4 molecules have been incubated under a range of conditions known to result in degradation of the therapeutic including varied pH, temperature, agitation, photo, and chemical stresses. Aggregation was measured using size-exclusion chromatography, and PTM levels were calculated using peptide mapping. By combining principal component analysis (PCA) with Raman spectroscopy and circular dichroism (CD) spectroscopy structural analysis we were able to separate proteins based on PTMs and degradation. Furthermore, by identifying key bands that lead to the PCA separation we could correlate spectral peaks to specific PTMs. In particular, we have identified a peak which exhibits a shift in samples with higher levels of Trp oxidation. Through separation of IgG4 aggregates, by size, we have shown a linear correlation between peak wavenumbers of specific functional groups and the amount of aggregate present. We therefore demonstrate the capability for Raman spectroscopy to be used as an analytical tool to measure degradation and PTMs in-line with therapeutic production.

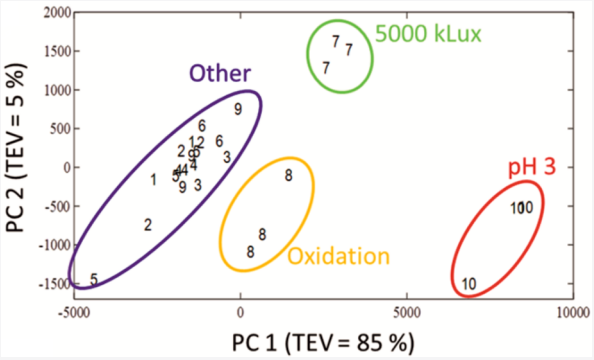

The pharmaceutical industry constantly strives for improved process analytical technology (PAT) to monitor and determine drug product quality. The need for enhanced analytics arises in turn from the demand of the health authorities, the largest two being the Food and Drug Administration and the European Medicines Agency, for greater pharmaceutical process understanding and in-depth product characterization.[1,2] Raman spectroscopy is an analytical technique that has been highlighted as a tool that could be used for in-line and possible online quality control monitoring in the largescale manufacture of drug molecules.[3−6] Raman spectroscopy is a vibrational technique that can provide molecular fingerprints using unique vibrations from different bonds within a molecular structure to build a picture of the functional groups and overall chemical arrangement. The technique is currently widely employed in the pharmaceutical sector to monitor chemical synthesis of drug molecules providing real-time critical quality attribute information.[7,8] However, biological therapeutics are typically complex, multi-domain globular proteins made up of hundreds of amino acids that can all influence the function of the protein. Monoclonal antibodies (mAbs) are now the biological therapeutic market leader,[9] but the structural complexity of these molecules increases the manufacturing cost due to a diverse range of possible degradation pathways. The possible batch heterogeneity therefore means extensive characterization is needed requiring time and expertise.[10−12] MAbs are typically ∼150 kDa and composed of multiple domains that result in the typical "Y" shape higher order structure. In general, the domains can be summarized as the Fab domain consisting of the F_V (Fab variable), C_H1 and C_L (heavy constant and light constant) domains, and the Fc region containing the C_H2 and C_H3 domains. In terms of degradation, it is well documented that mAbs are prone to aggregation and fragmentation, as well as a range of PTMs including oxidation of amino acids, induced by processing conditions.[13] The difficulty in avoiding these conditions comes from the fact that all mAbs have different propensities and mechanisms to aggregate or

Received: February 12, 2020
Accepted: July 1, 2020
Published: July 2, 2020

https://dx.doi.org/10.1021/acs.analchem.0c00627
Anal. Chem. 2020, 92, 10381−10389

fragment. Many stress induced aggregates can cause protein precipitation, although it is the soluble, subvisible aggregates that lead to immune responses. Fragmentation can also cause batch heterogeneity, as certain purification conditions can lead to nonenzymatic covalent bond breakage resulting in cleaving antibody domains from the intact mAb. Fragmentation is usually caused by hydrolysis of the peptide backbone, but is also common with certain amino acids, such as Asp, Gly, Ser, Thr, Cys, and Asn.[14] PTMs are chemical modifications to the amino acids that occur after expression of the antibodies. The most common PTMs include glycation, glycosylation, deamidation, and oxidation. These amino acid modifications can cause changes to the structure and physical properties of an antibody and may lead to a higher propensity to aggregate. PTMs can also significantly reduce the binding specificity of the F_V region when the modification occurs at a site that is important to binding, leading to reduced therapeutic efficacy. Current methodologies for assessing the amount of aggregation and PTMs, such as Size-Exclusion Chromatography (SEC) and peptide mapping, require sample collection and preparation and are therefore not suitable as a real-time PAT. Ideally industries that specialize in protein therapeutic processing need a PAT that can work in real-time, is used in-line with current industrial set-ups without sample preparation, and can be applied at different stages of the therapeutic manufacture without interfering with the process. This study investigates the sensitivity of Raman spectroscopy to measure degradation of an IgG4 therapeutic antibody, including fragmentation and aggregation, as well as PTMs such as oxidation and deamidation. A forced degradation study approach was used to induce degradation and PTMs using conditions known to cause measurable changes. Ten different conditions were chosen, including a reference sample that was stored at 4 °C. Aggregation and fragmentation was measured using SEC, and peptide mapping was used to quantify the induced PTMs. CD spectroscopy was used to determine tertiary and secondary structural information for the IgG4. CD spectral changes in the IgG4 degraded samples appeared to be minimal, however by combining PCA with CD, we were able to separate the samples based on PTMs and degradation using the loadings plots to identify the key spectral changes. This method was then applied to Raman spectroscopy and again PCA demonstrated the sensitivity and applicability of Raman to monitor degradation and PTMs for quality control of antibody therapeutics.

EXPERIMENTAL SECTION

IgG4 Forced Degradation. All forced degraded samples were made up to 3 mL at 25 mg mL^{-1} in the IgG4 UCB formulation buffer and incubated under varying conditions for 14 days unless otherwise stated. Heat degraded samples were incubated at 4, 40, and 50 °C. The 4 °C sample served as the control for degradation after 14 days. The pH degraded samples were adjusted to pH 3 with HCl and to pH 10 with NaOH. Both pH samples were incubated at 4 °C. Agitation degraded samples were placed on a 1400 rpm orbital shaker, at 25 °C. Deamidation conditions were created by buffer exchanging one sample into 1% ammonium bicarbonate buffer pH 8.1. pH was adjusted using NH_4OH 1 M. Oxidation conditions consisted of adding H_2O_2, 30% (w/w), to the IgG4 and formulation buffer to a final concentration of 1%. Both the deamidation and oxidation samples were stored at 4 °C. Light stressed samples were prepared by aliquoting IgG4 samples into quartz cuvettes and incubating in an Atlas Suntest XLS+ chamber with an intensity of 250 W/m^2 at 25 °C. The samples were exposed to 1000 and 5000 kLux·h of light, respectively, and were then incubated at 4 °C for the remainder of the 14 days.

Generation of IgG4 Aggregates for Separation. IgG4 was exposed to 5000 kLux·h of light at 25 °C. The samples were prepared as 45 mg mL^{-1} in formulation buffer.

Peptide Mapping. IgG4 was digested using trypsin, separated, analyzed by mass spectrometry, and compared to a database to give levels of modification. Details are given in the Supporting Information (SI).

Raman Spectroscopy. Raman measurements were undertaken on a Renishaw inVia Raman microscope (Renishaw Plc., Gloucestershire, U.K.) using a 785 nm laser. The experimental parameters used for all data collection were 100% laser power with a 10 s exposure and 20 accumulations, resulting in an overall acquisition time of 200 s per measurement. A 96 well quartz plate (Hellma) was used. The plate wells were randomized with 2 wells per sample. For each well, 4 repeats were obtained, leading to total of 8 repeats per sample. Raw and preprocessed spectra are shown in Figure S5.

RESULTS AND DISCUSSION

In order to determine the applicability of Raman spectroscopy for the PAT monitoring of antibody therapeutics we force degraded an IgG4 protein. Most antibody therapeutics are based on the IgG1 subclass, with IgG4 being the second most commonly used. IgG4 is known to be more susceptible to PTMs and degradation and therefore provided us with a wider range of samples to analyze.[15,16] The 10 different degradation conditions were selected to best represent current stability tests used within the pharmaceutical sector. The conditions are outlined in the Experimental Section.

Quantification of Aggregates and Fragments. SEC was used to determine the amount of aggregation and fragmentation that had occurred in each of the degradation conditions. The results are summarized in Figure S1. The control 4 °C sample shows that even the IgG4 held under nondegrading conditions for 14 days shows a small amount of aggregation (~1%). IgG4 irradiated with 5000 kLux·h of light at 300 to 800 nm shows the most degradation with 26% aggregation and 2% fragmentation. The oxidizing condition also led to 9% aggregation and 2% fragmentation. Incubation at pH 3 caused the most fragmentation (5%) with no aggregates present. The approximate masses derived from the reduced SDS page gels (Figure S2a) suggest that the fragments are ~30 kDa and therefore likely to be a fragment of the light chain (~25 kDa). The mass of the aggregates seen in the 5000 kLux·h condition are at least ~245 kDa (Figure S2) under nonreducing conditions. Under reduced conditions the size of the aggregates is significantly smaller, as the disulfide bond in the hinge region of the antibody is broken resulting in a fragment half the size of an intact IgG4. However, there are also bands at a higher MW than half an intact IgG4 suggesting that the aggregates are still intact when the disulfide bridge in the hinge region is broken. The remaining degradation conditions showed very similar aggregation levels as in the 4 °C control. The full SEC traces and analysis are shown in Figure S3 and Table S1.

Quantification of PTMs. To determine the extent of PTMs, peptide mapping of the IgG4 was used. This allowed an estimation of the quantity and identification of the chemical

https://dx.doi.org/10.1021/acs.analchem.0c00627
Anal. Chem. 2020, 92, 10381−10389

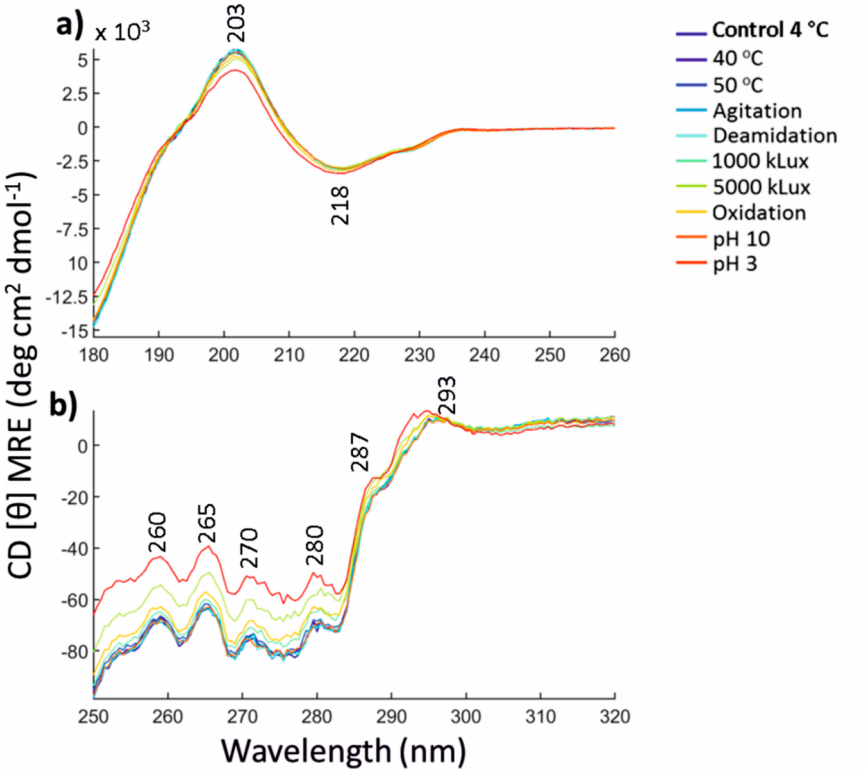

Figure 1. CD analysis of degraded IgG4 samples: (a) Far UV CD spectra and (b) Near UV CD spectra. Samples were diluted to 0.8 mg mL^{-1}. Data shown is an average of 9 spectra. *In the far UV CD Control 4 °C, 50 °C, and 1000 kLux·h is an average of 6 spectra due to three well repeats being outliers.

changes made to the amino acid side chains caused by the chosen conditions. The estimated PTM level for each site is shown as a percentage of the total ion count (TIC) of the most abundant charge state of the modified peptide against the corresponding unmodified peptide. It should be noted that mass spectrometry is a semiquantitative technique. These percentages are calculated from the ionization intensities reported by BioPharmaLynx for a particular modification within a peptide. The intensity of the modification is reported as a percentage of the total intensity of all variants of that peptide present from the tryptic digest. Often the unmodified peptides will have different ionization intensities compared with that of the modified and therefore the values are not necessarily an ultimate quantification. The full PTM report is in Tables S2 and S3.

The full PTM report are summarized in Figure S4. The control 4 °C sample shows the levels of post-translational modifications in an IgG4 sample after purification and stored under optimal conditions for this particular protein. In the control, oxidation of the Met, Trp, and His are 65%, 8%, and 3%, respectively. In general, Met usually oxidizes to form a sulfoxide and His has an addition of a carbonyl group to the imidazole ring to give 2-oxohistidine. Trp oxidation can be more complex as different products can be formed either through the addition of hydroxyl group to the benzene ring or a carbonyl to the indole.[17,18] Both heat incubated samples show similar levels of oxidation for all three amino acids but show an increase in deamidation as a function of temperature to 54% at 50 °C. Agitation shows little or no change compared to the control group. The light stressed samples both showed a large increase in the Met oxidation, rising to 100% with at least one oxidized Met in the 5000 kLux·h condition. Deamidation and Trp oxidation showed slight increases with longer duration of light, while His oxidation remained similar to that of the control. The oxidation samples showed an increase in oxidized Trp to 46% which was more than double that of any other sample and a 10-fold increase in the amount of His oxidation present to 30%. Oxidizing conditions also increased Met oxidation to 100%. The ease with which each amino acid side chain oxidizes can be summarized as Met > Trp > His, in agreement with previously published work on antibody oxidation.[17,19]

Structural Analysis Using Circular Dichroism. A typical IgG4 will be mainly β-sheet (40%) with little contribution from α-helices (4%).[20] CD is limited in terms of protein concentration and buffer and therefore the samples were diluted to 0.8 mg mL^{-1}.

Figure 1 shows the averaged CD spectra of three scans of three preparations of each degradation condition for the IgG4 in both (a) far and (b) near UV regions. CD spectra for β-structures are diverse, but in general it is expected that the spectra would have a maximum between 195−205 nm and a minimum at ∼218 nm. Figure 1a shows the far UV CD of all the averaged degradation conditions with maxima at 203 nm and minima at 218 nm from antiparallel β-sheets. The small negative band at ∼230 nm is thought to arise from aromatic side chains.[21] pH 3 stressed samples have secondary structures deviating from that of the control 4 °C sample. In particular, this sample has lower intensity at 203 nm and the peak at 218 nm has shifted to a lower wavelength suggesting that the protein may have lost some β-sheet structure and is more disordered than the other sample conditions. In Figure 1b the tertiary structure of the IgG4 under different degradation conditions can be seen. In the near UV region, it is more

https://dx.doi.org/10.1021/acs.analchem.0c00627
Anal. Chem. 2020, 92, 10381−10389

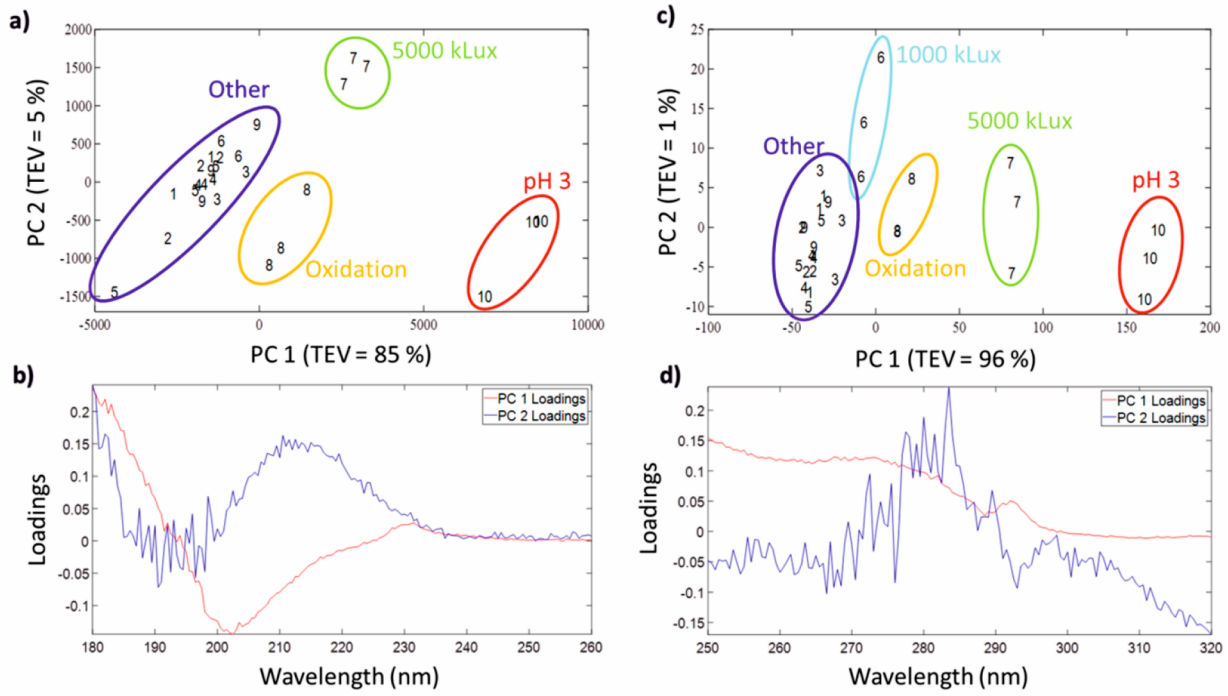

Figure 2. PCA and respective loadings plots for the far and near UV CD spectra of IgG4. (a) PCA of far UV CD, (b) loadings plot for far UV CD PCA, (c) PCA of near UV CD, and (d) loadings plot for near UV CD. TEV is the total explained variance of each PC. For each IgG4 degraded sample, three wells were aliquoted and measured in triplicate. Data are reported as an average of the triplicate repeats from one well. (1) Control 4 °C, (2) 40 °C, (3) 50 °C, (4) agitation, (5) deamidation, (6) 1000 kLux·h, (7) 5000 kLux·h, (8) oxidation, (9) pH 10, and (10) pH 3. *In the far UV CD 4 °C control, 50 °C, 1000 kLux·h is shown as an average of three repeats from two wells due to a well outlier from each.

difficult to relate exact wavelengths to specific structural components and instead ranges usually depict different amino acids groups in the tertiary structure. In terms of the amino acid side chains, Trp absorbs at ∼290 nm, Tyr at ∼280 nm, Phe at ∼260 nm, and disulfide bonds between 250−280 nm. To identify these smaller changes, we have used PCA, shown in Figure 2a,c. PCA reduces the dimensions of the data into a 2D plot which maximizes variation between the spectra using a scores plot. The loadings (Figures 2b and 2d) identify the key peaks or regions that lead to most separation in the data sets.

In Figure 2a, PC 1 accounts for 85% of the total explained variance (TEV), meaning the data are mainly separated across the *x*-axis. Replicates of the same conditions cluster close together showing that the measurements were reproducible. The pH 3, 5000 kLux·h, and oxidation conditions all fall within separate regions, showing that they form distinct structures. All other conditions cluster into "other" with the control conditions, suggesting that these conditions cause little change to the structure of the antibody. The loading plots shown in Figure 2b highlight the spectral regions that were most important to clustering in the PCA scores plot. PC 1 is separated on the intensity at 203 nm where it is decreased in conditions pH 3, 5000 kLux·h and oxidation, suggesting a change in the antiparallel β-sheet structure. The loadings plot in Figure 2d shows that an increasing peak at 290 nm is the main cause for the separation which signifies changes to Trp. There is also a difference in the baseline intensity of the absorbance across 250−280 nm suggesting changes in the disulfide bonding of the IgG4 seen in previous forced degradation studies.[22]

Structural Analysis Using Raman Spectroscopy. In general, secondary structural information can be gained from the Raman spectral region between 1700 and 1200 cm^{-1}, which includes the amide I, II, and III regions.[23] A full spectral assignment can be found in Table S6. Specifically, here is it possible to determine the α-helical, β-sheet, and disordered content. The main advantage of Raman is the quick spectral collection time and little to no sample preparation (water does not interfere); hence Raman is a strong candidate for real-time analysis of biotherapeutics production.[24,25] Figure 3a shows the Raman spectra as an average of 8 replicates. SI Figure S5a shows the raw data, and Figure S5b shows the buffer subtracted data highlighting the difference in the baseline across the degradation conditions. Figure S6 shows the buffer spectrum. Due to this difference in baselines and decreased intensity in samples with higher levels of aggregation, we have placed more emphasis on peak centers than the intensity. For all samples, the amide I peak is at 1666 cm^{-1} suggesting all samples have retained their β-sheet structure. All samples also retain a peak at 532 cm^{-1} suggesting that the disulfide bonding in the proteins is not affected by the degradation conditions. However, peak intensity ratios should be less affected by the buffer subtraction. A change in the peak intensity between two peaks, when compared across spectra, could therefore indicate real structural changes. In Figure 3a, the changes in peak ratios for the different degradation conditions are apparent in the amide III region between 1312 and 1334 cm^{-1} (assigned to Trp). This suggests real differences in the amide III and tertiary structure caused by the incubation conditions. Raman bands for the amino side chains are mainly located between 700 and 1000 cm^{-1}. As with the CD spectrum analysis, we have used PCA to look at differences between the spectra.

The PCA of the Raman data is shown in Figure 3b. The PCA shows clustering of the repeats from the same conditions,

https://dx.doi.org/10.1021/acs.analchem.0c00627
Anal. Chem. 2020, 92, 10381−10389

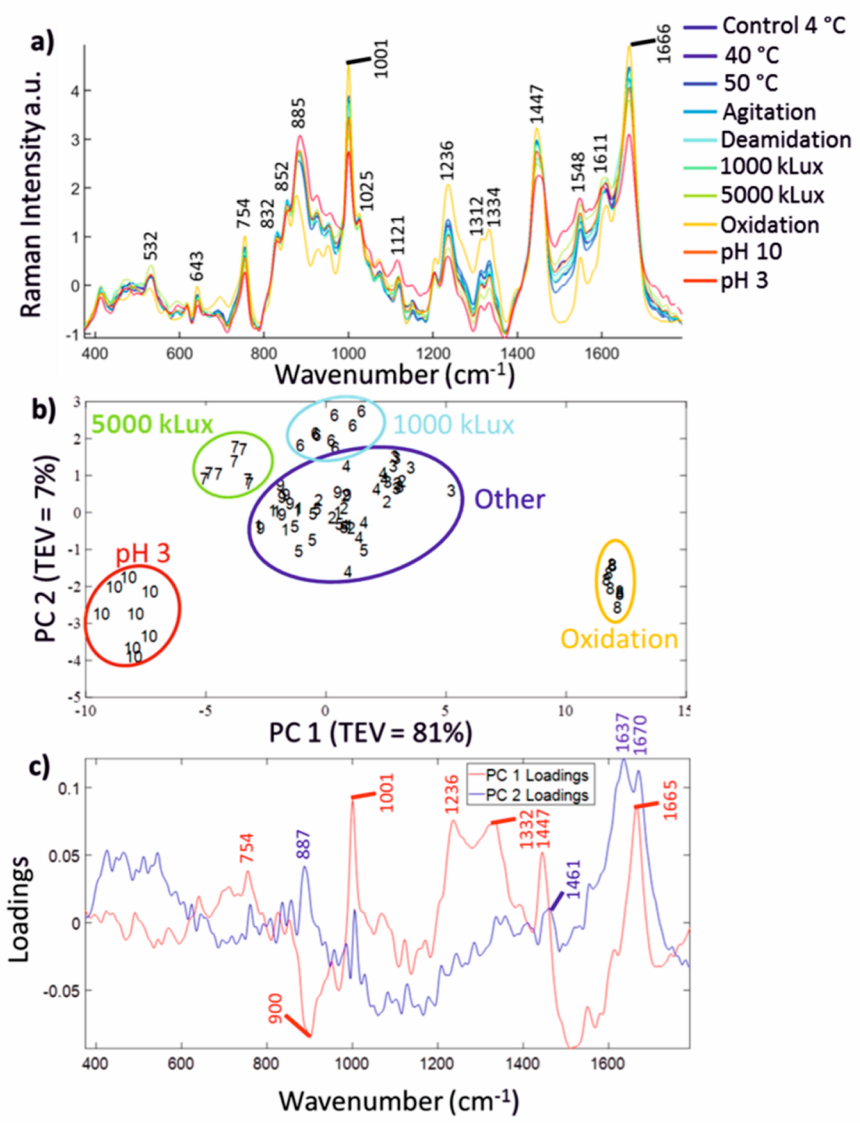

Figure 3. Raman spectra of degraded IgG4 samples with the respective PCA and loading plots. (a) Raman spectra (shown as an average of 8 repeats per condition), (b) PCA (showing 8 replicates individually), and (c) loadings plot showing PC 1 and PC 2. TEV is the total explained variance of each of PCs. (1) Control 4 °C, (2) 40 °C, (3) 50 °C, (4) agitation, (5) deamidation, (6) 1000 kLux·h, (7) 5000 kLux·h, (8) oxidation, (9) pH 10, and (10) pH 3.

meaning the data were reproducible. The samples that cluster separately to the control are oxidation, pH 3, 5000 kLux·h, and 1000 kLux·h. The remaining conditions were clustered with the control as "other". In Figure 3b both UV degrading conditions cluster above the "other" group, whereas the pH 3 and oxidation cluster below showing that different degradation conditions affect the antibodies in different ways. Figure 3c summarizes the loading plots of PC 1 and PC 2. Due to the baseline differences, the PC 1 is mainly attributed to signal intensities. PC 2 only accounts for 7% of the variance and although it does explain separation between the sample conditions it also highlights differences within the clusters especially of pH 3 and oxidation. The peaks at 1637 and 1670 cm^{-1} could be due to the buffer subtraction from samples with higher heterogeneity. Hence, we place higher emphasis on wavelengths of peak centers rather than intensities. When comparing both PC 1 and PC 2 of the Trp region at around 885 cm^{-1}, PC 1 shows an increase in a peak at 900 cm^{-1} for pH 3, while PC 2 has an increase in the peak intensity at 887 cm^{-1} for 5000 kLux·h and 1000 kLux·h, showing that the peak assigned to the Trp indole is important to the sample separation.[26,27] Figure 4a shows the average peak centers of the Trp peak for each degradation condition across the 8 sample repeats. The peak center positions show that the conditions that caused the largest shift in the Trp 885 cm^{-1} peak are oxidation, pH 3, 5000 kLux·h, and 1000 kLux·h, in agreement with the Raman PCA results. The oxidation samples show the largest shift to a lower wavenumber which suggests an increase in the strength of the indole N−H hydrogen bonding. In contrast, at pH 3, 5000 kLux·h, and 1000 kLux·h, there was a shift to a higher wavenumber indicating that Trp had weaker hydrogen bonding.[28]

The oxidation samples show the highest amount of Trp oxidation compared to all other conditions at 46% (Figure S5), which can be correlated to the largest shift in the Raman Trp peak in Figure 4. UV exposure to antibody therapeutics has been reported to follow specific Trp degradation pathways similar to that of H_2O_2 oxidation. For both H_2O_2 and UV

https://dx.doi.org/10.1021/acs.analchem.0c00627
Anal. Chem. 2020, 92, 10381−10389

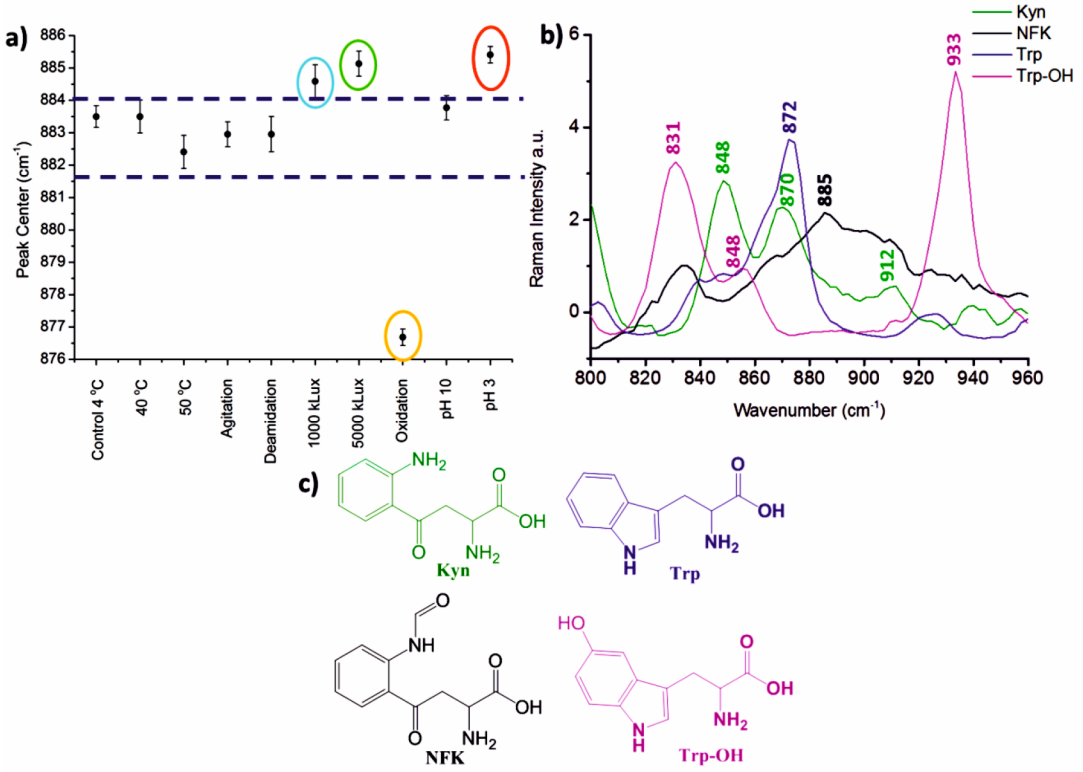

Figure 4. Peak centers of the Trp vibration in the force degraded samples and the possible degradation products. (a) Average peak center of the Trp vibration from 8 Raman repeats (colors highlight the clusters for comparison to PCA in Figure 5b. Error bars highlight the standard error (SE), (b) Trp vibrations of Trp, Kynurenine (Kyn), *N*-formylkynurenine, and 5-hydroxy Trp (Trp-OH); and (c) corresponding chemical structures.

induced Trp degradation, the most common products were hydroxytryptophan (OH-Trp), *N*-formylkynurenine (NFK), and kynurenine (Kyn) (Figure 4c).[17,29] The main difference between these degraded samples was the observed color change. For UV degraded proteins, the solutions turned yellow, whereas for H_2O_2, we observed no color change (Figure S7), suggesting there is a different mixture of Trp degradation products in the samples. The yellow color has previously been assigned primarily to the formation of Kyn and NFK.[17] Previously, a yellowing of mAb samples has been assigned to glycation; however, glycation levels are highest (9.7%) in the control 4 °C sample, which is colorless.[30,31] To rationalize the Trp indole peak shift we acquired spectra of the oxidized forms of Trp (Full spectra in Figure S8). The spectrum of dried Trp has a peak at 872 cm^{-1} (Figure 4b); however, in IgG4 in solution this peak is at ~884 cm^{-1}. These differences show that Trp peaks are sensitive to the environment; i.e., whether the side chains are in the hydrophobic core or exposed to solvent. We assume the shifts seen in the standard compounds apply to Trp in the protein. Kyn has a peak in the Raman spectrum at 870 cm^{-1}, a decrease in wavenumber compared to the control Trp. Kyn is also yellow. NFK is the only compound that has a peak at 885 cm^{-1}, as seen in both the 1000 kLux·h and 5000 kLux·h samples. We therefore suggest that the yellowing of the samples and increase in wavenumber in the 1000 kLux·h and 5000 kLux·h samples is due to formation of NFK. As there is also a shift to higher wavenumber in the pH 3 sample (5% fragmentation) there may be an environmental change within the protein structure. The oxidation sample shows a shift to a lower wavenumber in Figure 4b but no color change in Figure S7. Trp-OH is a colorless product and shows no peak around 870 cm^{-1}. The shift to a lower number can be assigned to the loss of the Trp band at 885 cm^{-1} and therefore leaving a peak at 876 cm^{-1} from the phosphate in the analysis buffer due to differences in the buffer subtraction of the degraded samples (Figure S5). This can be further seen in Table S4 where larger peaks shifts are seen in the buffer subtracted data compared to the data with no buffer subtraction suggesting that the phosphate peak may be masking the center of the Trp peak.

IgG4 Aggregate Separation. The forced degradation conditions produced a wide range of both degradation and PTMs resulting in complex mixtures. By far the largest problem in therapeutic degradation is the formation of aggregates that leads to the loss of material during downstream processing involving the mAbs being passed through a range of different columns to purify and remove waste from expression. IgG4 incubated under 5000 kLux·h light was therefore investigated further, as this condition produced the largest amount of aggregates (Figure S1). After incubation the sample was separated using SEC (Figure S9) into monomers, aggregate peak 1 (Fraction 2), and aggregate peak 2 (Fraction 3) which both resulted in a mixture of aggregates summarized in Table 1 below (separation and full SEC results are shown in SI Figures S10 and S11). Fragment concentrations were too low to be measured.

Each of the sample fractions shown in Table 1 was concentrated to 20 mg mL^{-1} and analyzed using the same Raman setup as described previously (section 2.4, Raman Spectroscopy). The average Raman spectrum across 8 repeats of each sample is shown in Figure 5a. Buffer was treated with 5000 kLux·h light before its spectrum was collected for subtraction (Figure S12). It was found that the higher quantity of the larger aggregates found in the sample correlated with an

https://dx.doi.org/10.1021/acs.analchem.0c00627
Anal. Chem. 2020, 92, 10381−10389

Table 1. Amount of Monomer and Aggregate in Each of the SEC Separated Fractions Determined by SE-UPLC[a]

SEC fraction	monomer (%)	aggregate 1 (%)	aggregate 2 (%)
1	100		
2	51	49	
3	17	33	50

[a]Analysis was carried out at 1 mg mL^{-1}.

increased baseline slope (Figure S13). We therefore focused on peak shifts rather than intensities. The peak at 532 cm^{-1} due to S−S bonds is present in all three samples suggesting that the disulfide bonding is still intact.[32,33] However, there is a small shift to a higher wavenumber in the Fraction 2 sample suggesting that although the S−S bonding is present there may be a small change in its environment or conformation. The amide I peak at 1666 cm^{-1} has not shifted, suggesting that aggregation is not significantly changing the overall secondary structure of the antibody.

The PCA plotted in Figure 5b shows the sample fractions are all spectrally distinct from each other. PC 1 accounts for 83% of the TEV and shows that fractions 2 and 3 are more spectrally similar to each other than to the monomer. Although the repeats from the same fraction cluster, they also show some separation on PC 2, accounting for only 12% of the TEV, which is possibly due to baseline differences from the well repeats. The separation of samples within the same fraction increases with higher levels of larger aggregates in the sample suggesting that the heterogeneity of the sample increases with aggregation, leading to difficulty in buffer subtraction. Figure 5c summarizes the loadings for PC 1. In general, PC 1 resembles an antibody spectrum as the main differences in the PCA are the peak intensities. However, a few peaks can be seen to differ in position compared to the spectrum in Figure 5a. This shift is particularly apparent at 901, 1123, and 1448 cm^{-1}. Figure S14 shows the peak shifts across the three sample fractions. Figure S14a shows the peak centers at ∼1121 cm^{-1}, 8b ∼ 1450 cm^{-1} and 8c ∼ 890 cm^{-1}. An increase in the Trp wavenumber from monomer to Fraction 3 suggests that the

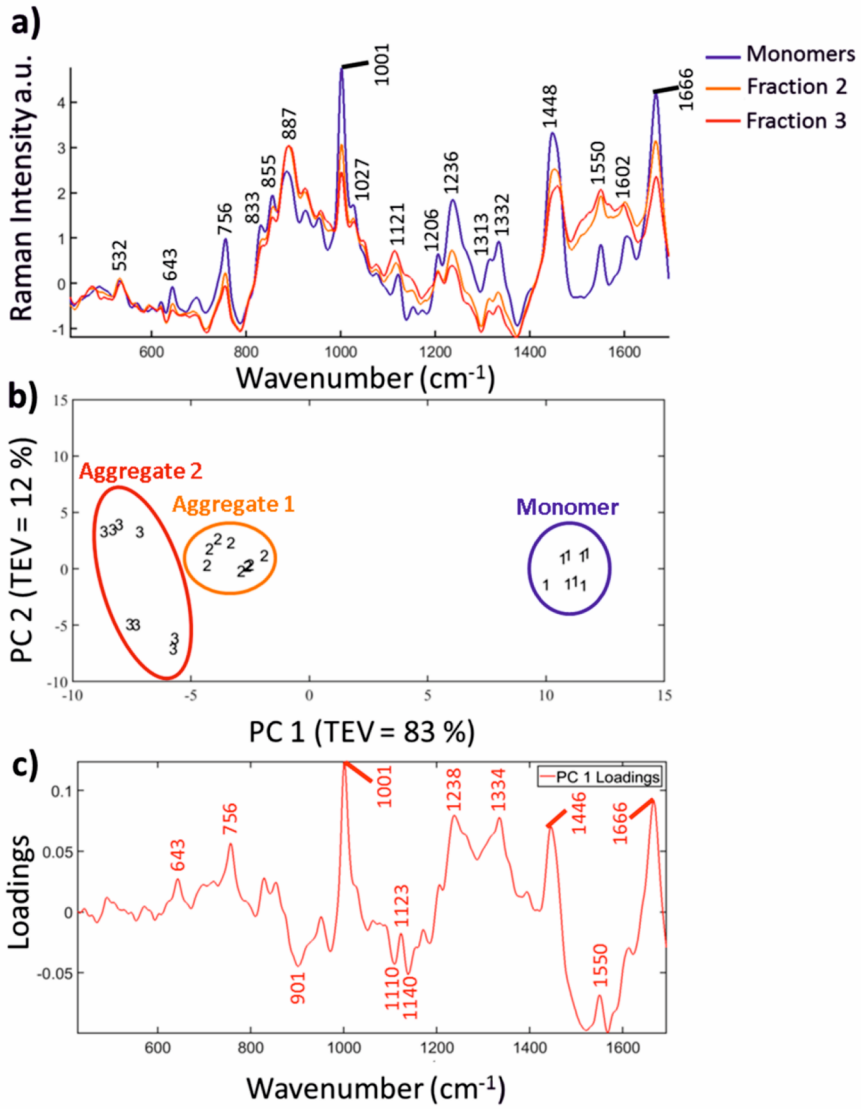

Figure 5. Raman spectra of separated aggregate species of IgG4 samples from exposure to UV light with the respective PCA and loadings plots. (a) Raman spectra (shown as an average of 8 repeats), (b) PCA (showing 8 replicates individually), and (c) loadings plot showing PC 1. (1) Fraction 1 (monomer), (2) Fraction 2, and (3) Fraction 3. TEV is the total explained variance of each PC.

https://dx.doi.org/10.1021/acs.analchem.0c00627
Anal. Chem. 2020, 92, 10381−10389

strength of the N−H hydrogen bonding decreases as the protein aggregates. The peak at 1450 cm^{-1} is assigned to C−H deformation.[23,34,35] This is specifically vibrations from CH_2 and CH_3 groups. From the Monomer to Fractions 2 and 3, the peak shifts to a higher wavenumber suggesting a change in the environment of the C−H bonding and possibly the protein structure. In most amino acid side chains, there is a CH_2, making explaining the shift difficult. The peak centered at 1121 cm^{-1} has been assigned to C−N bonding which is mainly found in the protein backbone.[35,36] From Monomer to Fraction 3, the peak center of the C−N vibrations is shifted to a lower wavenumber. Again, as the C−N bond is seen throughout the protein backbone, it is difficult to correlate the peak shift with a specific structural change, but it does show that there are differences in the overall protein structure. Figure 5a shows peak ratio differences between 1313 and 1332 cm^{-1} (also seen in Figure 3a) in which the ratio decreases from monomers to dimers to aggregates. This suggests a structural change within the amide III region and tertiary structure of the antibody. These Raman spectral shifts have also been reported in a recent paper by Zhang et al.,[37] where samples of varying mAb aggregate levels were generated and analyzed using Raman spectroscopy and chemometrics, such as two-dimensional correlational spectroscopy (2DCOS) and support vector machines (SVM). Similarly to our results, they found changes in Amide II, CH deformation region, of the Raman spectrum in aggregated samples. Unfortunately, due to buffer excipients, they were not able to analyze peaks below 1160 cm^{-1}, such as the 1121 and 885 cm^{-1} shown in this work. The combination of these results suggests peak shifts measured in aggregates, especially in the Amide II region, may be applicable to aggregates in other types of mAb therapeutics.

CONCLUSIONS

We have demonstrated, for the first time, the ability of Raman spectroscopy to differentiate between force degraded samples of an IgG4 with differing PTMs, fragmentation, and aggregation. Furthermore, we have shown the ability of Raman to distinguish between samples of monomers and mixed aggregate species. Structural differences between the force degraded samples are small and difficult to distinguish when interpreting conventional CD and Raman spectra. However, by combining spectroscopic analysis with chemometrics, such as PCA, we are able to draw out subtle structural differences. Furthermore, by using the peak shifts highlighted in the loadings plots we were able to assign spectral features to specific PTMs and degradation types that were used by the PCA to separate the data. Thus, the loadings identified key peaks that could be used to monitor structural changes in mAbs for quality control. Both the PCAs of the CD and Raman data showed that the 5000 kLux·h, pH 3 and oxidation conditions gave samples that differed most to the control. Specifically, in Raman, we saw peak shifts in the N−H vibration (~885 cm^{-1}) of the indole of Trp, indicating hydrogen bonding and environmental changes. Peak shifts were assigned to different degradation products of Trp caused by oxidation. IgG4 incubated with H_2O_2 has the highest amount of Trp oxidation (46%) but remains colorless when degraded. Under UV light, at 1000 kLux·h and 5000 kLux·h, the sample become increasingly yellow with a longer UV exposure. However, the total oxidation is less than half that seen with H_2O_2 (20% and 13%, respectively). Using the color changes reported previously in literature and the standard spectra of the degradation products, we have assigned the peak shifts to different degradation products of Trp. Our investigations show that a decrease in the wavenumber at ~885 cm^{-1} is indicative of Trp-OH (colorless), whereas an increase shows NFK formation (yellow). These peak shifts have been further extended to an investigation into the sensitivity of Raman to detect aggregates where monomers and aggregates were separated by size. The Raman analysis identified peak shifts at 885, 1121, and 1450 cm^{-1} attributed to Trp, C−N backbone, and C−H, respectively. Both the Trp and C−H vibrations shift to a higher wavenumber with increasing size and amounts of aggregates in the sample. The C−N backbone shows a decrease in wavenumber from monomer to more aggregates in the sample. Overall these findings suggest a backbone structural change and a change of the environment to the Trp as protein aggregates allowing for discrimination between samples. Biological therapeutics often show only subtle changes or structural rearrangements that are difficult to detect in such a large molecule. The development of PAT testing for biological therapeutics is therefore complex and difficult to implement. These results therefore provide the first demonstration of the applicability and sensitivity of Raman spectroscopy to detect structural changes in a range of force degraded mAbs. The spectral characteristics attributed to these structural changes can be exploited in developing in-line analytics for therapeutic mAb quality control.

ASSOCIATED CONTENT

Supporting Information

The Supporting Information is available free of charge at https://pubs.acs.org/doi/10.1021/acs.analchem.0c00627.

Figure S1, SEC results; Figure S2, approximate masses derived from the reduced SDS page gels; Figure S3 and Table S1, full SEC traces and analysis; Figure S4, full PTM report; Tables S2 and S3, full PTM report; Figure S5, raw data; Figure S6, buffer spectrum; Figure S7, UV degraded proteins; Figure S8, Trp indole full spectra; Figure S9, sample separation using SEC; Figures S10 and S11, separation and full SEC results; Figure S12, buffer spectrum; Figure S13, larger aggregates correlated with an increased baseline slope; and Figure S14, peak shifts across the three sample fractions (PDF)

AUTHOR INFORMATION

Corresponding Author

Andrew J. Doig − *Division of Neuroscience and Experimental Psychology, School of Biological Sciences, Faculty of Biology, Medicine and Health, University of Manchester, Manchester M13 9PT, United Kingdom;* orcid.org/0000-0003-0346-2270; Email: andrew.doig@manchester.ac.uk

Authors

Bethan S. McAvan − *School of Chemistry, Manchester Institute of Biotechnology, University of Manchester, Manchester M1 7DN, United Kingdom*

Leo A. Bowsher − *UCB Celltech, UCB Pharma, Limited, Berkshire SL1 3WE, United Kingdom*

Thomas Powell − *UCB Celltech, UCB Pharma, Limited, Berkshire SL1 3WE, United Kingdom;* orcid.org/0000-0002-8308-6510

John F. O'Hara − *UCB Celltech, UCB Pharma, Limited, Berkshire SL1 3WE, United Kingdom*

https://dx.doi.org/10.1021/acs.analchem.0c00627
Anal. Chem. 2020, 92, 10381−10389

Mariangela Spitali − *UCB Celltech, UCB Pharma, Limited, Berkshire SL1 3WE, United Kingdom*
Royston Goodacre − *Department of Biochemistry, Institute of Integrative Biology, University of Liverpool, Liverpool L69 7ZB, United Kingdom;* orcid.org/0000-0003-2230-645X

Complete contact information is available at: https://pubs.acs.org/10.1021/acs.analchem.0c00627

Funding
BBSRC CASE award with UCB Pharma BB/L014734/1.

Notes
The authors declare no competing financial interest.

■ ACKNOWLEDGMENTS

The project is funded by the BBSRC and UCB Pharma as a CASE partner. All mAb samples were kindly donated by UCB Pharma. We would like to thank Michael Knight, UCB Pharma, Ltd., Slough, for help performing SEC and the separation of the IgG4 aggregates.

■ ABBREVIATIONS USED

mAb	monoclonal antibody
CD	Circular Dichroism
SEC	Size Exclusion Chromatography
PTM	Post Translational Modification
TEV	Total Explained Variance
PC	Principal Component
PCA	Principal Component Analysis
C_H2	Constant heavy domain 2
C_H3	Constant heavy domain 3
F_v	Fragment variable
C_H1	Constant heavy domain 1
C_L	Constant light domain
DSP	downstream processing
2DCOS	two-dimensional correlational spectroscopy

■ REFERENCES

(1) FDA, Guidance for Industry PAT—A Framework for Innovative Pharmaceutical Development, Manufacturing, and Quality Assurance, 2004, www.fda.gov/regulatory-information/search-fda-guidance-documents/pat-framework-innovative-pharmaceutical-development-manufacturing-and-quality-assurance (accessed July 16, 2020).
(2) European Medicines Agency. Committee for Medicinal Products for Human Use (CHMP) Guideline on similar biological medicinal products containing monoclonal antibodies-nonclinical and clinical issues, (2012). www.ema.europa.eu (accessed June 17, 2019).
(3) Esmonde-White, K. A.; Cuellar, M.; Uerpmann, C.; Lenain, B.; Lewis, I. R. *Anal. Bioanal. Chem.* **2017**, *409*, 637−649.
(4) Nagy, B.; Farkas, A.; Gyürkés, M.; Komaromy-Hiller, S.; Démuth, B.; Szabó, B.; Nusser, D.; Borbás, E.; Marosi, G.; Nagy, Z. K. *Int. J. Pharm.* **2017**, *530*, 21−29.
(5) Li, M. Y.; Ebel, B.; Paris, C.; Chauchard, F.; Guedon, E.; Marc, A. *Biotechnol. Prog.* **2018**, *34*, 486−493.
(6) Rüdt, M.; Briskot, T.; Hubbuch, J. *J. Chromatogr. A* **2017**, *1490*, 2−9.
(7) De Beer, T.R.M.; Bodson, C.; Dejaegher, B.; Walczak, B.; Vercruysse, P.; Burggraeve, A.; Lemos, A.; Delattre, L.; Heyden, Y. V.; Remon, J.P.; et al. *J. Pharm. Biomed. Anal.* **2008**, *48*, 772−779.
(8) Eliasson, C.; Macleod, N. A.; Jayes, L. C.; Clarke, F. C.; Hammond, S. V.; Smith, M. R.; Matousek, P. *J. Pharm. Biomed. Anal.* **2008**, *47*, 221−229.
(9) Biologics Market By Types (Monoclonal Antibodies, Therapeutic Proteins And Vaccines), By Trends, By Regions And By Key Players - Global Forecast To 2021. The Business Research Company. www.thebusinessresearchcompany.com/report/biologics-market (accessed July 16, 2020).
(10) Wang, W.; Singh, S.; Zeng, D. L.; King, K.; Nema, S. *J. Pharm. Sci.* **2007**, *96*, 1−26.
(11) Li, F.; Lee, B.; Zhou, J.; Tressel, T.; Yang, X. *BioProcess. J.* **2006**, *5*, 16−25.
(12) Waghmare, J.; Mark, S.; Juan, W.; Claire, C.; Scanlan, R. *Biopharm Int.* **2014**, *1*, 42−44.
(13) Elgundi, Z.; Reslan, M.; Cruz, E.; Sifniotis, V.; Kayser, V. *Adv. Drug Delivery Rev.* **2017**, *122*, 2−19.
(14) Vlasak, J.; Ionescu, R. *MAbs.* **2011**, *3*, 253−63.
(15) Ishikawa, T.; Ito, T.; Endo, R.; Nakagawa, K.; Sawa, E.; Wakamatsu, K. *Biol. Pharm. Bull.* **2010**, *33*, 1413−1417.
(16) Neergaard, M. S.; Nielsen, A. D.; Parshad, H.; Van De Weert, M. *J. Pharm. Sci.* **2014**, *103*, 115−127.
(17) Li, Y.; Polozova, A.; Gruia, F.; Feng, J. *Anal. Chem.* **2014**, *86*, 6850−7.
(18) Amano, M.; Kobayashi, N.; Yabuta, M.; Uchiyama, S.; Fukui, K. *Anal. Chem.* **2014**, *86*, 7536−7543.
(19) Folzer, E.; Diepold, K.; Bomans, K.; Finkler, C.; Schmidt, R.; Bulau, P.; Huwyler, J.; Mahler, H. C.; Koulov, A. V. *J. Pharm. Sci.* **2015**, *104*, 2824−2831.
(20) Micsonai, A.; Wien, F.; Kernya, L.; Lee, Y.-H.; Goto, Y.; Réfrégiers, M.; Kardos, J. *Proc. Natl. Acad. Sci. U. S. A.* **2015**, *112*, E3095−103.
(21) Venyaminov, S.Y.; Yang, J.T. Determination of Protein Secondary Structure. In *Circ. Dichroism Conform. Anal. Biomol.*; Springer: Boston, MA, 1996; pp 69−107 DOI: 10.1007/978-14757-2508-7_3.
(22) Barnett, G. V.; Balakrishnan, G.; Chennamsetty, N.; Meengs, B.; Meyer, J.; Bongers, J.; Ludwig, R.; Tao, L.; Das, T. K.; Leone, A.; Kar, S. R. *J. Pharm. Sci.* **2018**, *107*, 2559−2569.
(23) Rygula, A.; Majzner, K.; Marzec, K. M.; Kaczor, A.; Pilarczyk, M.; Baranska, M. *J. Raman Spectrosc.* **2013**, *44*, 1061−1076.
(24) Westley, C.; Fisk, H.; Xu, Y.; Hollywood, K. A.; Carnell, A. J.; Micklefield, J.; Turner, N. J.; Goodacre, R. *Chem. - Eur. J.* **2017**, *23*, 6983−6987.
(25) Herrington, W. F.; Singh, G. P.; Wu, D.; Barone, P. W.; Hancock, W.; Ram, R. J. *Sci. Rep.* **2018**, *8*, 5089.
(26) Miura, T.; Takeuchi, H.; Harada, I. *Biochemistry* **1988**, *27*, 88−94.
(27) Hédoux, A.; Guinet, Y.; Paccou, L. *J. Phys. Chem. B* **2011**, *115*, 6740−6748.
(28) Miura, T.; Takeuchi, H.; Harada, I. *J. Raman Spectrosc.* **1989**, *20*, 667−671.
(29) Simat, T. J.; Steinhart, H. *J. Agric. Food Chem.* **1998**, *46*, 490−498.
(30) Yuk, I. H.; Zhang, B.; Yang, Y.; Dutina, G.; Leach, K. D.; Vijayasankaran, N.; Shen, A. Y.; Andersen, D. C.; Snedecor, B. R.; Joly, J. C. *Biotechnol. Bioeng.* **2011**, *108*, 2600−2610.
(31) Butko, M.; Pallat, H.; Cordoba, A.; Yu, X. C. *Anal. Chem.* **2014**, *86*, 9816−9823.
(32) Ettah, I.; Ashton, L. *Antibodies* **2018**, *7*, 24.
(33) Van Wart, H. E.; Scheraga, H. A. *J. Phys. Chem.* **1976**, *80*, 1823−1832.
(34) Schneider, B.; Štokr, J.; Schmidt, P.; Mihailov, M.; Dirlikov, S.; Peeva, N. *Polymer* **1979**, *20*, 705−712.
(35) De Gelder, J.; De Gussem, K.; Vandenabeele, P.; Moens, L. *J. Raman Spectrosc.* **2007**, *38*, 1133−1147.
(36) Sato, E. T.; Martinho, H. *Biomed. Opt. Express* **2018**, *9*, 1728−1734.
(37) Zhang, C.; Springall, J. S.; Wang, X.; Barman, I. *Anal. Chim. Acta* **2019**, *1081*, 138−145.